Journal of
Synchrotron
Radiation

ISSN 0909-0495

Received 21 March 2011
Accepted 7 November 2011

Increase of lifespan for glioma-bearing rats by using minibeam radiation therapy

Yolanda Prezado,[a]*‡ Sukhena Sarun,[a]‡ Silvia Gil,[a,b] Pierre Deman,[a,c,d] Audrey Bouchet[a,e] and Geraldine Le Duc[a]

[a]ID17 Biomedical Beamline, European Synchrotron Radiation Facility, 6 Rue Jules Horowitz, BP 220, 38043 Grenoble Cedex, France, [b]Centre d'Estudis en Biofísica, Unitat de Biofísica, Faculty of Medicine, Universitat Autonoma de Barcelona, Spain, [c]Inserm, U836, Equipe 6, BP 170, 38042 Grenoble Cedex, France, [d]Université Joseph-Fourier, BP 51, 38041 Grenoble Cedex, France, and [e]Grenoble Institute of Neurosciences, Team 7, Grenoble, France. E-mail: prezado@esrf.fr

This feasibility work assesses the therapeutic effectiveness of minibeam radiation therapy, a new synchrotron radiotherapy technique. In this new approach the irradiation is performed on 9L gliosarcoma-bearing rats with arrays of parallel beams of width 500–700 μm. Two irradiation configurations were compared: a lateral unidirectional irradiation and two orthogonal arrays interlacing at the target. A dose escalation study was performed. A factor of three gain in the mean survival time obtained for some animals paves the way for further exploration of the different possibilities of this technique and its further optimization.

Keywords: brain tumors; minibeam radiation therapy; preclinical trials.

1. Introduction

The goal of radiotherapy is to deposit a therapeutic radiation dose in the tumor without exceeding the tolerances of the nearby healthy tissue. There are some particularly radioresistant tumors, such as gliomas, for which the dose-response curves for tumor control and normal tissue complications lie in close proximity to the dose distributions achievable in clinics nowadays. This results in only palliative treatments. This limitation is especially severe in children, owing to the high risk of complications in the development of the central nervous system. The management of tumors close to an organ of risk, such as the spinal cord, is also very limited. In order to widen the therapeutic window for gliomas, two new radiotherapy techniques are under development at the biomedical beamline of the European Synchrotron Radiation Facility (ESRF): microbeam radiation therapy (MRT) and, more recently, minibeam radiation therapy (MBRT).

These techniques combine the use of submillimetric field sizes and a spatial fractionation of the dose. The beam widths range from 25 to 100 μm in the case of MRT and from 500 to 700 μm in MBRT, exploring the limits of what it is called the dose-volume effect: the smaller the field size, the higher the tolerances of the healthy tissues (Curtis, 1967; Lawrence *et al.*, 2010). Very high doses ($\geq$50 Gy) are delivered in one fraction by using the mean energy of arrays of intense parallel X-ray beams at around 100 keV (Siegbahn *et al.*, 2006). The interbeam separation is 200 μm or 400 μm in the case of MRT and 600 μm in MBRT.

During the last two decades several experiments have shown the sparing effect of the healthy tissues provided by MRT on the central nervous system of several animal models (Slatkin *et al.*, 1995; Laissue *et al.*, 1999, 2001; Dilmanian *et al.*, 2001; Regnard *et al.*, 2008; Serduc *et al.*, 2008). In addition, a remarkable preferential tumoricidal effect at high doses has been observed (Laissue *et al.*, 1998, 1999; Dilmanian *et al.*, 2002, 2003; Smilowitz *et al.*, 2006; Miura *et al.*, 2006; Regnard *et al.*, 2008; Serduc *et al.*, 2009).

The thin microbeams (and their associated small beam spacing) need high dose rates, only available at synchrotrons nowadays. This is due to the fact that, since microbeams are closely packed, it is important that the tissue/target does not move during the irradiation owing to the cardiosynchronous pulsations (Poncelet *et al.*, 1992). Such motions would smear out the dose in between the microbeams and therefore would jeopardize the tissue sparing effect of the microbeams. This limits their widespread clinical implementation. In addition, the high lateral scattering produced by beam energies higher than 200 keV would lead to the loss of the healthy tissue sparing (Prezado *et al.*, 2009*a*). The requirement of low-energy beams limits the dose penetration to the tissue. To overcome these difficulties, Dilmanian *et al.* (2006) proposed the so-called MBRT. They have hypothesized that beams as thick as 0.68 mm keep (part of) the sparing effect (Dilmanian *et al.*, 2006) observed in MRT, supporting a potential application of minibeams to treat tumors with minimal damage to the

‡ These authors contributed equally to this work.

surrounding healthy tissue. In addition, from MRT preclinical studies there are indications that a wider beam results in a higher tumoricidal effect (Serduc *et al.*, 2009). Moreover, in MBRT the use of higher beam energies is feasible (Prezado *et al.*, 2009*b*), resulting in a lower entrance dose to deposit the same integral dose in the tumor. It requires less precision of targeting and synchronization than microscopic beams. The clinical implementation of interlaced MBRT (Dilmanian *et al.*, 2006) producing a broad beam at the target is technically much less challenging than with thinner beams. The dose profiles of minibeams are not as vulnerable as those of microbeams to beam smearing from cardiac pulsations; therefore high dose rates are not needed and it is conceptually possible to extend this technique by using modified X-ray equipment.

For the aforementioned reasons, a new method has been developed and tested at the ESRF ID17 biomedical beamline to produce the minibeam patterns (Prezado *et al.*, 2009*c*). It utilizes a specially developed white-beam chopper. The method offers an excellent reliability and allows for an easy control of all the parameters which are essential for the general safety of the treatment. Following the results of Dilmanian *et al.* (2006), at the ESRF the minibeams are produced with a beam thickness of 640 μm and a center-to-center distance of 560 μm. This method was applied to treat the rat 9L glioma model, commonly used in MRT. Two different MBRT geometry configurations were studied: (i) a single array of minibeams (unidirectional); (ii) two orthogonal arrays interlacing at the target, such that a quasi-homogeneous dose distribution in the tumor is achieved while the healthy tissue still benefits from the spatial fractionation of the submillimetric beams.

The survival lifespan of the 9L glioma rat model after each of these irradiation configurations will be compared.

2. Materials and methods

2.1. Radiation source

The ESRF is one of three synchrotrons in the world with the highest energy and brilliance. At the ID17 biomedical beamline the X-ray source consists of two wigglers with periods 15 cm and 12.5 cm and a maximum magnetic field of 1.6 T. It is located 40 m from the patient positioning system and delivers high-intensity kilovoltage-energy X-ray beams. The X-ray energy spectrum after filtering ranges from about 50 to 500 keV, with a mean energy around 100 keV (Siegbahn *et al.*, 2006). The maximum field dimensions achievable are 3 mm height and 36 mm width. Since the beam height is very small, the animals are scanned vertically through the beam. The synchrotron beams at the target position have negligible divergence (allowing the production of sharply defined beam edges in tissue) and high flux (exceeding the flux of a tungsten-anode X-ray tube by five orders of magnitude). A more detailed technical description of the beamline layout can be found in the work of Renier *et al.* (2008).

2.2. Dosimetry

The dose deposited on the rat brain was assessed both theoretically (Monte Carlo simulations) and experimentally. The Monte Carlo code used was *PENELOPE 2006* (Salvat *et al.*, 2006). In this code all relevant physical processes for photons (photoelectric effect, Rayleigh and Compton scattering) as well as for electrons (elastic scattering and ionization) are considered. Dose distributions (peak and valley doses) were assessed both in water and rat phantoms. Experimental validation of the calculations was performed by using HD-810 radiochromic films placed at different depths in a water-equivalent phantom (Prezado *et al.*, 2009*c*). The absolute dose for a 2 cm × 2 cm seamless field at 1.0 cm depth was measured using an ionization chamber (PTW 31002) in the same water-equivalent phantom. The dose measured in this broad field configuration was converted to peak doses at 1.0 cm depth by using the phantom scatter factors calculated by Monte Carlo simulations and verified experimentally by using gafchromic films. The peak dose at 1 cm depth in water was then converted to dose deposited at 1 cm depth in the rat phantom by means of a precalculated (Monte Carlo) calibration factor.

2.3. Intracerebral gliosarcoma model in rat

The 9L gliosarcoma cell line (Coderre *et al.*, 1994; Régnard *et al.*, 2008) was established by Benda *et al.* (1971). Cells were grown with complete medium at 310 K. Anesthetized male Fisher 344 rats (180–250 g; Charles River, L'Arbresle, France) were placed on a stereotactic head holder (model 900; David Kopf Instruments, Tujunga, USA). 10^4 cells were suspended in 1 μl DMEM with antibiotics (1%) and then injected using a Hamilton syringe through a burr hole in the right caudate nucleus (9 mm anterior to the ear-bars, *i.e.* at the bregma site, 3.5 mm lateral to the midline, 5.5 mm depth from the skull) (Kobayashi *et al.*, 1980; Paxinos & Watson, 1986).

At all stages of the experiment (innoculation and irradiation) the rats were anesthetized with 4% isoflurane inhalation followed by an intraperitoneal injection of xylazine/ketamine (64.5/5.4 mg kg^{-1}). All operative procedures related to animal care strictly conformed to the Guidelines of the French Government with licenses 380825 and B3818510002 and were reviewed by the Internal Evaluation Committee for Animal Welfare and Rights of the ESRF.

2.4. Radiation exposure

Thirty-six tumor-bearing rats were treated ten days after tumor implantation as follows: (i) six rats were not irradiated and were used as control; (ii) ten rats were irradiated unidirectionally by the lateral direction (right to left) with an escalation in doses; the irradiation was performed with an array of six horizontal minibeams, 640 μm wide and 1120 μm center-to-center distance, covering an area of 8 mm × 8 mm; (iii) 20 rats were irradiated by using two orthogonal arrays of interlaced minibeams, one of them in the lateral direction (right to left), the other in the craneo-caudal direction, also covering an area of 8 mm × 8 mm.

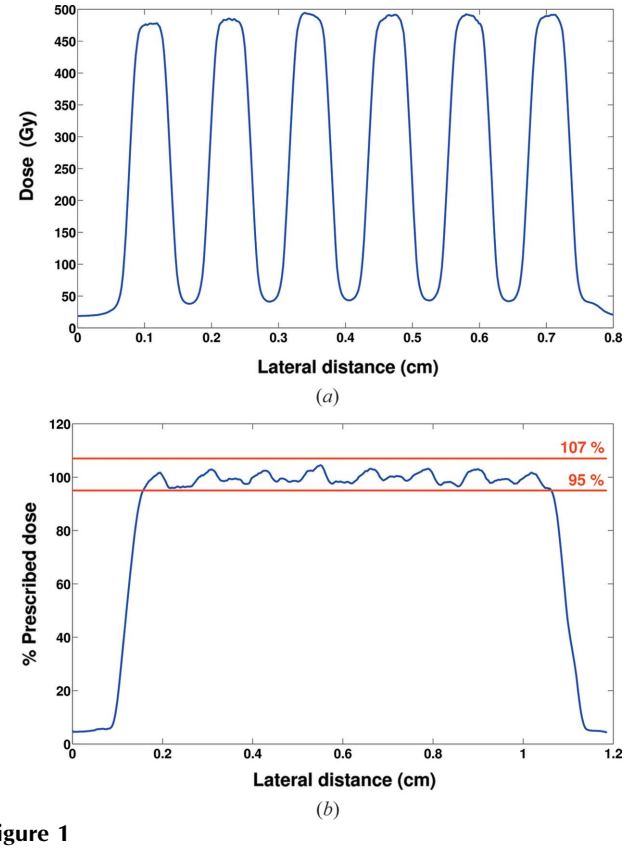

Figure 1
Dose distributions at a depth of 1 cm in a solid water phantom for a unidirectional irradiation (*a*) and for an interlaced configuration (*b*). The distributions were measured by using gafchromic films.

The size of the tumor, assessed by MRI the day before irradiation, was 2 mm × 3 mm.

A dose escalation study was performed. The dose prescriptions (at 1 cm depth) were:

(i) Unidirectional (lateral) irradiation: 100 Gy peak dose (9 Gy valley dose) (n = 3), 150 Gy peak dose (13 Gy valley dose) (n = 3) and 180 Gy peak dose (16 Gy valley dose) (n = 4). The doses were chosen such that they were within safe limits observed in the work of Dilmanian *et al.* (2006).

(ii) Interlaced irradiation: 40 Gy (n = 6), 53 Gy (n = 5), 70 Gy (n = 6) and 100 Gy (n = 3).

Figs. 1(*a*) and 1(*b*) show the dose distributions at 1 cm depth in a solid water phantom, measured using gafchromic films, for the unidirectional and interlaced irradiations, respectively. In the latter, the dose distribution fulfills the requirements to be considered as homegeneous: the dose in the target fits within 95–107% of the prescribed dose (ICRU, 1993).

For irradiation the rats were positioned on a home-made holder and fixed by the teeth and ears on top of a three-axis κ-type goniometer (Huber, Germany) (Renier *et al.*, 2008). For each rat an HD 810 radiochromic film was positioned in front of the head. Inspection of the films ensured the quality of the irradiation.

2.5. Survival analysis

The clinical status of the rats was checked twice a week. At a later tumor stage, some rats were euthanized by intra-cardiac injection of sodium pentobarbital at less than 1 day before their anticipated death as judged by clinical signs (Laissue *et al.*, 1998). Some of them were found dead. The time between implantation and death was recorded as the survival time. The median survival time post-implantation was calculated and Kaplan Meier survival data were plotted *versus* time after tumor implantation. The increase in lifespan in percent (%ILS) characterizes the difference between median survival time for treated and untreated rats divided by the median survival time for untreated rats. The survival curves were compared using the log-rank test between the irradiated groups and the controls.

2.6. Histologic analysis

The irradiated rat brains were sampled and frozen in formalin after the death/euthanasia of the rats. Transversal brain sections of size 10 µm were cut at 253 K using a cryotome (Microm HM560, France) and stained according to the standard haematoxylin-eosin (HE) procedure (Regnard *et al.*, 2008).

2.7. Magnetic resonance imaging (MRI)

The rats receiving interlaced irradiation (100 Gy) underwent an MRI examination on day 21 after implantation.

Images were acquired using a 7 T Bruker imaging system coupled with a bird-cage radiofrequency coil by applying (i) the T_2-weighted Turbo RARE SE sequence [echo time (TE) = 11 ms, repetition time (TR) = 4000 ms]; (ii) the T_1-weighted Turbo RARE SE sequence (TE = 4.85 ms, TR = 800 ms) after gadolinium chelate injection through the tail vein.

3. Results

3.1. Survival curves

The survival curves and the detailed values of the mean survival time (MeST) and increase in life span (ILS) are reported in Fig. 2 and Table 1, respectively. The control

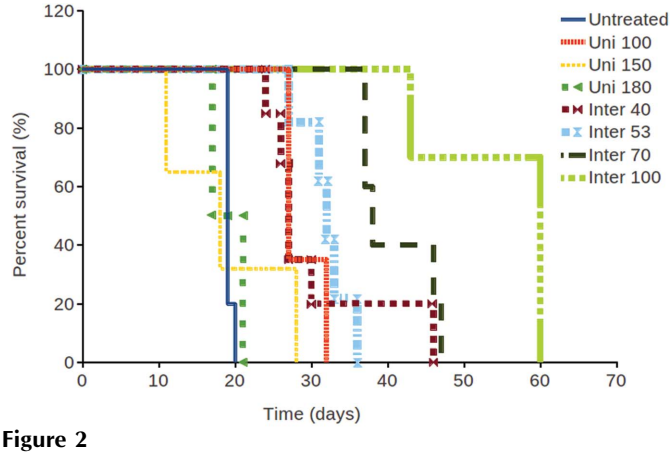

Figure 2
Survival curves (as a function of time) of 9L gliosarcoma-bearing rats for different doses. The response of both the control rats (CTRL) and the rats receiving one fraction minibeam radiation therapy in unidirectional and interlaced configurations are shown.

Table 1
Mean survival time (MeST) and the corresponding standard error of the mean (SEM), increase of life span (ILS), significance *versus* control, and *p* values for the two irradiation geometries and dose groups.

Uni refers to unidirectional irradiation, Inter to interlaced configuration. S refers to 'Significant', NS to 'Not Significant'.

Series	No. of rats	Dose (Gy)	MeST (SEM) (days)	ILS (%)	Significance *versus* CTRL	*p* value
CRTL	6	N/A	N/A	19.0 (0.3)	N/A	N/A
Uni 100	3	100	27 (2)	42	S	0.0082
Uni 150	3	150	18 (4)	−5	NS	
Uni 180	3	180	20 (3)	5	NS	
Inter 40	6	40	27 (1)	42	S	0.0008
Inter 53	4	53	32 (2)	68	S	0.0016
Inter 70	6	70	38 (2)	100	S	0.0016
Inter 100	3	100	60 (6)	215	S	0.0082

(CTRL) rats exhibited a mean survival time of 19 days. The difference between survival curves for the irradiated series *versus* the control series was significant for most of the curves except for the unidirectional irradiation at 150 Gy and 180 Gy, which showed no increase in life span. The best MeSTs were obtained when performing interlaced irradiation at 70 Gy and 100 Gy, showing an increase in life span of 100% and 215%, respectively.

3.2. Follow-up of the animals

A few days before death the rats showed typical signs of the presence of tumors, *e.g.* chromodacryorrhea, tarnished hairs, prostration, weakness and difficulty in feeding.

3.3. H/E coloration and MRI images

The recurrence of tumor growth was observed in all of the rats and is evident on the HE staining. For example, Fig. 3 shows how a tumor invaded a hemisphere in the brain of one of the rats that received 100 Gy interlaced irradiation. For all of the rats a very large tumor was observed, either invading the right hemisphere of the brain or spreading to the margin of the left hemisphere at the rat death. The MRI images were taken 21 days after implantation. Aedema is observed in the T_2-weighted sequence while disruption of the blood brain barrier appears in the T_1-weighted sequence with gadolinium contrast, indicating the presence of a tumor.

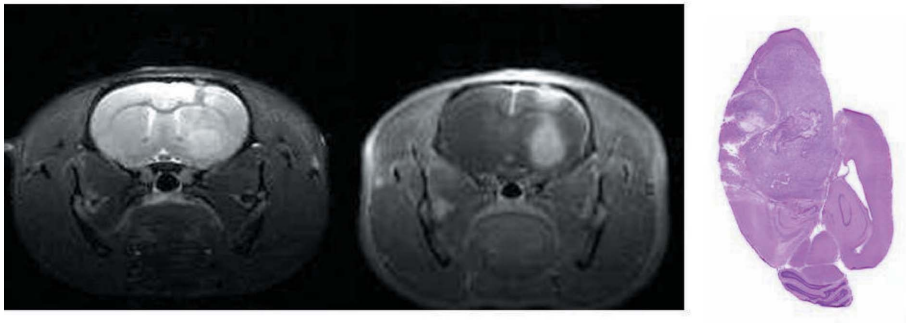

Figure 3
Left: T_2-weighted image. Center: T_1-weighted sequence with gadolinium contrast. MRI was performed on day 21 after tumor implantation. The presence of the tumor in the right hemisphere is observed. Right: an example of an H/E-stained brain cut of series Inter 100. The tumor occupies the right hemisphere completely.

4. Discussion

The beam type (photons, electrons, protons, *etc.*), beam quality and dose delivery method (fractionation scheme, dose rate, spatial distribution, *etc.*) have a direct impact on the biological effect of the radiation (Steel *et al.*, 2002). The modification of any of the aforementioned parameters implies a different biological response and it might lead to a shift of the healthy tissue complication probability curve to higher doses, opening in this way the therapeutic window for gliomas. This idea is the basis of two new radiotherapy techniques: microbeam radiation therapy (MRT) and, more recently, minibeam radiation therapy (MBRT). These techniques present distinct features with respect to conventional radiotherapy methods:

(i) Submillimetric field sizes are used, exploring the limits of what it is called the dose-volume effect.

(ii) The dose is spatially fractionated: very high doses ($\geq$50 Gy) are delivered in one fraction by using arrays of intense parallel beams. The interbeam separation is 200 µm or 400 µm in the case of MRT and 600 µm in MBRT.

(iii) The X-ray energy spectrum employed ranges from 50 to 500 keV, with a mean energy at around 100 keV (Siegbahn *et al.*, 2006).

(iv) Extremely high dose rates ($\geq$5000 Gy s^{-1}) have been used to date in order to provide a fast irradiation.

The preclinical studies performed in MRT up to now indicate that a change of these four parameters leads to an opening of the therapeutic window for gliomas. Although the biological mechanisms playing a role in MRT irradiation are not fully known yet, the healthy tissue sparing effect in the beam paths has been attributed to rapid biological repair of the microscopic lesions by the minimally irradiated cells contiguous to the irradiated tissue slices (Serduc *et al.*, 2006). This reparation effect has also been observed in experiments with high-energy photons (Hopewell & Trott, 2000). In order to explain this phenomenon, a stem cell depletion hypothesis has been formulated: for each organ there exists a limiting critical volume which can be repopulated by a single surviving stem cell and for which damage can be repaired by repopulation (Yaes & Kalend, 1988).

However, the widespread implementation of MRT is restrained owing to technical difficulties and the requirement of very high dose rates, only available at synchrotrons nowadays. MBRT has the potential to overcome these limitations.

In this study the effectiveness of MBRT for the treatment of 9L glioma was investigated. Tumor-bearing rats were irradiated using two different geometries, unidirectional and inter-

laced configurations, with an escalation of doses. The MeST of CTRL rats of 19 days is in agreement with similar protocols (Regnard *et al.*, 2008). The unidirectional series do not provide a significant improvement with respect to untreated controls. This might indicate that the valley doses in the target (maximum 12 Gy for 180 Gy peak dose) are not high enough. This is coherent with the minimum lethal dose for cells found while performing *in vitro* studies (20 Gy valley dose) (Sarun *et al.*, 2010). Moreover, the fact that rats in the groups at 150 and 180 Gy died within a few days after irradiation might point at healthy tissue toxicity.

In contrast, interlaced irradiation provides a significant increase in both MeST and ILS with respect to the controls. This gain augments as a function of the dose delivered. The highest increment ($\times 3$) in MeST was obtained with an interlaced irradiation for the highest dose (100 Gy), reaching an ILS of 215%. This MeST (60 days) is comparable with that obtained using the standard ESRF interlaced MRT configuration (65 days) (Bouchet *et al.*, 2010). Additionally, the mean survival time observed by depositing 20 Gy by broad-beam irradiation (unidirectional) under the same experimental conditions was 24 days (n = 12) (detailed results not shown).

While the remarkable healthy tissue sparing in MRT has already been clearly demonstrated by numerous experiments, in MBRT the first experiments performed by Dilmanian *et al.* (2006) indicate that minibeams keep part of the healthy tissue sparing as shown by the thinner beams. However, further histological analysis is needed for confirmation. Despite probably losing in normal tissue sparing, MBRT is technically easier to implement than MRT and it offers the possibility of being extended towards hospitals with cost-effective X-ray equipment.

The results obtained in this study could be improved by:

(i) The use of image guidance. Owing to the fact that the irradiations were performed using anatomical landmarks for target positioning, the field sizes used were large in comparison with the target size. This led to an increase in healthy tissue damage around the target, especially in the interlaced irradiation geometry. Moreover, since image guidance was not used, part of the tumor might have escaped from the irradiated area.

(ii) Employing new combinations of chemo-radiotherapy.

(iii) Exploiting the dose enhancement effect in the tumor by using high-atomic-number elements (Prezado *et al.* 2009*a*).

Theoretical advantages of MBRT over the existing clinical radiotherapy and radiosurgery methods might include the following:

(i) Owing to its lower impact on the non-targeted tissue, it might allow the use of high potentially curative doses in those clinical cases in which cure is not possible today.

(ii) It might allow re-treatment of the central nervous system months or years after the initial treatment(s).

(iii) The reduced penumbras (≤ 100 µm) make MBRT the best candidate for what is starting to be called micro-radiosurgery for the treatment of illnesses such as epilepsy (Anschel *et al.*, 2007), without significant secondary effects. In addition, it could be used for the treatment of tumors close to an organ at risk, such as the spinal cord.

5. Conclusions

Minibeam radiation therapy is an innovative synchrotron radiation therapy technique with the potential of application outside synchrotron sources. In this work the effectiveness of a single-fraction MBRT to treat glioma-bearing rats has been assessed. Two different irradiation configurations (unidirectional and interlaced) and different doses have been studied. While unidirectional irradiation showed no benefit with respect to untreated controls, the interlaced geometry provided a significant enhancement of MeST (a factor of three with respect to controls) and in life span (215%). These results provide evidence of the feasibility of this new technique for treating gliomas. Improvement of the outcome is expected by using image guidance, chemoradiotherapy *etc.* in future studies.

The authors warmly acknowledge the granted beam time at the ID17 biomedical beamline at the ESRF. The authors would like to thank the support of the ID17 and the animal facility staff at the ESRF. The authors especially thank A. Bravin for the reading of this manuscript, C. Le Clec'h and R. Serduc for help with the histology analysis.

References

Anschel, D. J., Romanelli, P., Benveniste, H., Foerster, B., Kalef-Ezra, J., Zhong, Z. & Dilmanian, F. A. (2007). *Minim. Invas. Neurosurg.* **50**, 43–46.

Benda, P., Someda, K., Messer, J. & Sweet, W. (1971). *J. Neurosurg.* **84**, 310–323.

Bouchet, A., Lemasson, B., Le Duc, G., Maisin, C., Bräuer-Krisch, E., Siegbahn, E. A., Renaud, L., Khalil, E., Rémy, C., Poillot, C., Bravin, A., Laissue, J. A., Barbier, E. L. & Serduc, R. (2010). *Intl J. Radiat. Oncol. Biol. Phys.* **78**, 1503–1512.

Coderre, J. A., Button, T. M., Micca, P. L., Fisher, C. D., Nawrocky, M. M. & Liu, H. B. (1994). *Intl J. Radiat. Oncol. Biol. Phys.* **30**, 643–652.

Curtis, H. J. (1967). *Radiat. Res. Suppl.* **7**, 250–257.

Dilmanian, F. A., Button, T., Le Duc, G. *et al.* (2002). *Neuro Oncol.* **4**, 26–38.

Dilmanian, F. A., Morris, G., Le Duc, G. *et al.* (2001). *Cell. Mol. Biol.* **47**, 485–493.

Dilmanian, F. A., Morris, G. M., Zhong, N., Bacarian, T., Hainfeld, J. F., Kalef-Ezra, J., Brewington, L. J., Tammam, J. & Rosen, E. M. (2003). *Radiat. Res.* **159**, 632–641.

Dilmanian, F. A., Zhong, Z., Bacarian, T., Benveniste, H., Romanelli, P., Wang, R., Welwart, J., Yuasa, T., Rosen, E. M. & Anschel, D. J. (2006). *Proc. Natl. Acad. Sci. USA*, **103**, 9709–9714.

Hopewell, J. W. & Trott, K.-R. (2000). *Radiother. Oncol.* **56**, 283–288.

ICRU (1993). *Prescribing, Recording and Reporting Photon Beam Therapy*, ICRU report 50. Washington DC: International Commission on Radiation Units and Measurements.

Kobayashi, N., Allen, N., Clendenon, N. R. & Ko, L.-W. (1980). *J. Neurosurg.* **53**, 808–815.

Laissue, J. A. *et al.* (2001). *Proc. SPIE*, **4508**, 65–73.
Laissue, J. A., Geiser, G., Spanne, P. O., Dilmanian, F. A., Gebbers, J. O., Geiser, M., Wu, X. Y., Makar, M. S., Micca, P. L., Nawrocky, M. M., Joel, D. D. & Slatkin, D. N. (1998). *Intl J. Cancer*, **78**, 654–660.
Laissue, J. A., Lyubimova, N., Wagner, H.-P., Archer, D. W., Slatkin, D. N., Di Michiel, M., Nemoz, C., Renier, M., Brauer, E, Spanne, P. O., Gebbers, J.-O., Dixon, K. & Blattmann, H. (1999). *Proc. SPIE*, **3770**, 38–45.
Lawrence, Y. R., Li, X. Q., El Naqa, I., Hahn, C. A., Marks, L. B., Merchant, T. E. & Dicker, A. P. (2010). *Intl J. Radiat. Oncol. Biol. Phys.* **76**, S20–S27.
Miura, M., Blattmann, H., Bräuer- Krisch, E., Bravin, A., Hanson, A. L., Nawrocky, M. M., Micca, P. L., Slatkin, D. N. & Laissue, J. A. (2006). *Br. J. Radiol.* **79**, 71–75.
Paxinos, G. & Watson, C. (1986). Editors. *The Rat Brain in Stereotaxic Coordinates.* New York: Academic.
Poncelet, B. P., Wedeen, V. J., Weisskopf, R. M. & Cohen, M. S. (1992). *Radiology*, **85**, 645–651.
Prezado, Y., Fois, G., Le Duc, G. & Bravin, A. (2009*a*). *Med. Phys.* **36**, 3568–3574.
Prezado, Y., Renier, M. & Bravin, A. (2009*c*). *J. Synchrotron Rad.* **16**, 582–586.
Prezado, Y., Thengumpallil, S., Renier, M. & Bravin, A. (2009*b*). *Med. Phys.* **36**, 4897–4902.
Régnard, P., Le Duc, G., Brauer, E., Tropes, I., Siegbahn, E. A., Kusak, A., Clair, C., Bernard, H., Dallery, D., Laissue, J. A. & Bravin, A. (2008). *Phys. Med. Biol.* **53**, 861–878.
Renier, M., Brochard, Th., Nemoz, C., Requardt, H. *et al.* (2008). *Eur. J. Radiol.* **68**S, 147–150.
Salvat, F., Fernández-Varea, J. M. & Sempau, J. (2006). *PENELOPE-2006. A Code System for Monte Carlo Simulation of Electron and Photon Transport.* Issy-les-Moulineaux: OECD Nuclear Energy Agency.
Sarun, S., Gil-Duran, S., Fauquette, W. *et al.* (2010). *Radiother. Oncol.* **96**, S255.
Serduc, R., Bouchet, A., Bräuer-Krisch, E., Laissue, J. A., Spiga, J., Sarun, S., Bravin, A., Fonta, C., Renaud, L., Boutonnat, J., Siegbahn, E. A., Estève, F. & Le Duc, G. (2009). *Phys. Med. Biol.* **54**, 6711–6724.
Serduc, R., van de Looij, Y., Francony, G., Verdonck, O., van der Sanden, B., Laissue, J., Farion, R., Bräuer-Krisch, E., Siegbahn, E. A., Bravin, A., Prezado, Y., Segebarth, C., Rémy, C. & Lahrech, H. (2008). *Phys. Med. Biol.* **53**, 1153–1166.
Serduc, R., Vérant, P., Vial, J. C., Farion, R., Rocas, L., Remy, C., Fadlallah, T., Brauer, E., Bravin, A., Laissue, J., Blattmann, H. & van der Sanden, B. (2006). *Intl J. Radiat. Oncol. Biol. Phys.* **64**, 1519–1527.
Siegbahn, E. A., Stepanek, J., Bräuer-Krisch, E. & Bravin, A. (2006). *Med. Phys.* **33**, 3248–3259.
Slatkin, D. N., Spanne, P., Dilmanian, F. A., Gebbers, J. O. & Laissue, J. A. (1995). *Proc. Natl Acad. Sci. USA*, **92**, 8783–8787.
Smilowitz, H. M., Blattmann, H., Bräuer-Krisch, E., Bravin, A., Di Michiel, M., Gebbers, J. O., Hanson, A. L., Lyubimova, N., Slatkin, D. N., Stepanek, J. & Laissue, J. A. (2006). *J. Neurooncol.* **78**, 135–143.
Steel, G. G., Adams, G. E. & Horwich, A. (2002). *Basic Clinical Radiobiology.* London: Edward Arnold.
Yaes, R. J. & Kalend, A. (1988). *Intl J. Radiat. Oncol. Biol. Phys.* **14**, 1247–1259.